



## ORIGINAL ARTICLE

# Characterization of activated carbon prepared by phosphoric acid activation of olive stones



S.M. Yakout \*, G. Sharaf El-Deen

Hot Labs Center, Atomic Energy Authority, P.C. 13759 Cairo, Egypt

Received 26 June 2011; accepted 10 December 2011

Available online 22 December 2011

## KEYWORDS

Activated carbon;  
Yield;  
Olive stones;  
Phosphoric acid;  
Porous texture

**Abstract** The effects of activating agent concentration on the pore structure and surface chemistry of activated carbons derived from olive stone with chemical activation method using phosphoric acid as the activating agent were studied. Mass changes associated with the impregnation, carbonization and washing processes were measured. With  $H_3PO_4$  dilute solutions (60, 70, and 80 wt%  $H_3PO_4$ ), the loading of substance on CS increases with concentration. The concentration of the  $H_3PO_4$  solution seems to control the processes of impregnation, carbonization and washing in the preparation of AC from olive stones by  $H_3PO_4$  chemical activation. ACs have been characterized from the results obtained by  $N_2$  adsorption at 77 K. Moreover, the fractal dimension ( $D$ ) has been calculated in order to determine the AC surface roughness degree. Optimal textural properties of ACs have been obtained by chemical activation with  $H_3PO_4$  80 wt.%. The BET surface areas and total pore volumes of the carbons produced at  $H_3PO_4$  80 wt.% are  $1218 \text{ m}^2/\text{g}$  and  $0.6 \text{ cm}^3/\text{g}$ , respectively.

© 2011 Production and hosting by Elsevier B.V. on behalf of King Saud University. This is an open access article under the CC BY-NC-ND license (<http://creativecommons.org/licenses/by-nc-nd/3.0/>).

## 1. Introduction

Olive is the most extensively cultivated fruit crop in the world. Olive cultivation is particularly widespread throughout the Mediterranean region and plays an important role in its rural economy, local heritage, and environment protection. The largest producing countries are located in the Mediterranean and Middle East regions providing 98% of the total cul-

tivated surface area, and 99% of the total olive fruit production (Niaounakis and Halvadakis, 2006). The world production of olives, for the year 2007, was 17.4 Mton, of which 12.6 Mton came from Europe (FAOSTAT, 2009).

Activated carbon is also among the potential conversions, with applications in the removal of dyes, odors, tastes, and contaminants, in water purification and other decontamination processes (Matos et al., 2010). Olive stone is a lignocellulosic material, with hemicellulose, cellulose and lignin as the main components. Olive stones could be a very adequate feedstock to obtain active carbons with good adsorptive properties and hardness, which could be of interest in future environmental protection programs.

Activated carbon (AC) is widely used on an industrial scale as an adsorbent mainly in the purification/separation of liquids and gases and also as a catalyst and catalyst support

\* Corresponding author. Tel.: +20 0482807763.

E-mail address: [sobhy.yakout@gmail.com](mailto:sobhy.yakout@gmail.com) (S.M. Yakout).

Peer review under responsibility of King Saud University.



(Olivares-Marin et al., 2006). Furthermore, newer applications are ever emerging, particularly those concerning environmental protection and technological development.

There are basically two methods for activated carbons' production: physical and chemical activations. Physical activation includes the carbonization of the starting material and the activation of the carbonize using steam and carbon dioxide. In the chemical activation method, phosphoric acid and zinc chloride are used for the activation of lignocellulosic materials, which have not been carbonized previously; whereas metal compounds such as potassium hydroxide are used for the activation of coal precursors or chars. When compared to zinc chloride, phosphoric acid is the most preferred because of the environmental disadvantages associated with zinc chloride. Problems of corrosion and inefficient chemical recovery are also associated with it. Moreover, the carbons obtained using zinc chloride cannot be used in pharmaceutical and food industries as they may contaminate the product (Prahas et al., 2008). Although potassium hydroxide develops large microporosity, the yield of activated carbon impregnated by potassium hydroxide is lower than those activated with zinc chloride or phosphoric acid, and at high temperature, i.e.  $> \pm 650$  °C, the carbon content is less than fixed carbon in the initial precursor. The presence of metallic potassium will intercalate to the carbon matrix (Prahas et al., 2008), yielding lower yield of activated carbon, less than the carbon content of the raw material.  $H_3PO_4$  is the most widely used impregnation agent. Using this substance, most of the numerous studies carried out so far on the preparation of AC have focused on the influence of concentration of the impregnation solution and soaking temperature on the porous structure. Because of the highly polar character of  $H_3PO_4$  and hence the control of the physical and chemical interactions occurring in the bulk of the solution and with the substratum during the impregnation treatment, the solution concentration is likely to be the primary factor of the activation process. Here, dilute and concentrated solutions of  $H_3PO_4$  are used in the impregnation of an AC precursor, the influence of phosphoric acid concentration on the loading of  $H_3PO_4$  is investigated. This work deals with the influence of the treatment methods of olive stones and SEOP on the structure and surface properties of the produced activated carbons.

## 2. Materials and methods

### 2.1. Active carbon preparation

As indicated above, olive stones (OS) were used as a precursor. OS as received was ground, dried and sieved, and only the fraction of particle sizes comprised between 1 and 2 mm was selected for the preparation of activated carbons. Approximately, 50 g of conditioned OS was impregnated with 200 ml of phosphoric acid solutions with concentrations of 60, 70 and 80 wt.% mixture stirred at 85 °C, maintaining for 4 h to ensure the access of  $H_3PO_4$  to the interior of the olive stones. After mixing, carbonization of acid-impregnated OS was carried out in a stainless steel reactor provided with gas inlet and outlet, which was placed in a vertical cylindrical furnace. The temperature within the furnace was first calibrated and the length and position of the constant temperature hot zone determined. Heating from room temperature to the maximum heat treatment temperature 500 °C (i.e., carbonization

temperature) in inert atmosphere of nitrogen (flow rate = 200 mL/min. The heating rate was 3 °C/min and holding time 2 h). After heating, the system was cooled down to room temperature under the same flow of nitrogen and the product obtained was washed with distilled water until pH 6 was reached in the residual liquid and finally oven-dried at 120 °C. OS6, OS7, OS8 were used as a label for activated carbon prepared from olive stones at  $H_3PO_4$  60wt.%, 70wt.%, 80wt.% concentrations, respectively.

Low temperature-ramping rate of 3 °C/min was used in this stage to minimize the temperature difference between the furnace chamber and activation mixture as well as maintain the mixture at a specific temperature range for enough time so that perceptible activation extent could be obtained and an optimized activation temperature range could be determined.

### 2.2. Active carbon characterization

Nitrogen adsorption/desorption isotherms were measured at 77 K on an automatic adsorption instrument (Quantachrome Instruments, Model Nova1000e series, USA) in relative pressure ranging from  $10^{-6}$  to 0.999. Prior to the measurement, all the samples were crushed and powdered to shorten the time required for reaching equilibrium in the isotherm study and degassed at 250 °C under nitrogen flow for 16 h.

The nitrogen adsorption–desorption isotherms were used to determine the following parameters: specific surface area SBET (according to the BET equation), total pore volume  $V_{tot}$  (calculated from the nitrogen uptake at relative pressure of 0.95), total micropore volume  $V_{micro}$ , according to simplified equations (Mehandjiev et al., 1994; Nickolov and Mehandjiev, 2000, 1995), total mesopore volume  $V_{mes}$  (determined by subtracting the micropore volume from the total pore volume), mean pore radius  $r_p$  (calculated using the total pore volume and the BET surface area, assuming a cylindrical pore model), the micropore size distribution parameter  $X_o$  (the half-width of the distribution curve maximum) was calculated according to simplified equation of the Horvath–Kawazone (HK) method (Ustinov and Do, 2002).

The fractal dimension is often used as an index of roughness or irregularity of the surface of ACs (Diaz-Diez et al., 2004) among other materials. In this work, the fractal dimension was determined by applying the FHH (Frenkel–Halsey–Hill) equation (Halsey, 1948) to the adsorption isotherm.

Apparent (bulk) density of all samples was calculated as the ratio between weight and volume of packed dry material.

The FTIR spectra of the samples were recorded between 4000 and 450  $cm^{-1}$  in a Perkin-Elmer 1720 spectrometer. Pellets were prepared by thoroughly mixing carbon and KBr at the 1:400 carbon/KBr weight ratio in a small size agate mortar. The resulting mixture was compacted in a Perkin-Elmer manual hydraulic press at 10 ton for 3 min.

The sample morphology was observed using a scanning electron microscope (SEM) model JEOL 5400. The specimens for SEM observation were prepared by depositing the fibers onto specimen-stubs with conductive double sticky copper tapes, and then sputter-coating (model Polaron SC7640, Quorum Technologies Ltd., UK) the sample surface with Au–Pd to prevent electrical charging during examination. Imaging was done in the high vacuum mode under an accelerating voltage of 15 kV, using secondary electrons.

### 3. Result and discussion

#### 3.1. Yield of activated carbon

The nomenclature, operation conditions, density and yield of the different samples prepared by the method of chemical activation with phosphoric acid are summarized in Table 1. The results obtained clearly show that, as expected, as  $\text{H}_3\text{PO}_4$  concentration increases the total yield of the process decreases. Essentially, Olive stone is a lignocellulosic material, with hemicellulose, cellulose and lignin as the main components. In activation or carbonization, these polymeric structures decompose and liberate most of the non-carbon elements, mainly hydrogen, oxygen and nitrogen in the form of liquid (called as tars) and gases, leaving behind a rigid carbon skeleton in the form of aromatic sheets and strips. In other words, the reaction of lignocellulose with phosphoric acid begins as soon as the components are mixed, the acid first attacks hemicellulose and lignin because cellulose is known to be more resistant to acid hydrolysis (Jagtoyen and Derbyshire, 1998). Here the acid will hydrolyze glycosidic linkages in lignocellulosic and cleave aryl ether bond in lignin. These reactions are accompanied by further chemical transformations that include dehydration, degradation, and condensation. As the acid concentration increases, the aromatic condensation reactions also take place among the adjacent molecules, which result in the evolution of gaseous products from the hydroaromatic structure of carbonized char leading to decreased yield of carbon (Timur et al., 2006). Also, here the excess phosphoric acid will promote gasification of char and increased the total weight loss of carbon. The same result was also observed by other researchers (Jagtoyen and Derbyshire, 1998; Timur et al., 2006).

As seen from table, the bulk density decreases with increasing acid concentration. This means that increasing acid concentration results in carbon richer in carbon and is more porous. Also, as seen the weight after impregnation increases as the acid concentration increases. This means that the weight of residue after phosphoric acid impregnation shows a great influence of the  $\text{H}_3\text{PO}_4$  concentration on the amount of  $\text{H}_3\text{PO}_4$  loaded on OS.

From these results it is clear that with the concentrated  $\text{H}_3\text{PO}_4$  solution a synergic effect occurred in the impregnation of OS which was likely connected with the strong dependence of the molecular association of  $\text{H}_3\text{PO}_4$  on the concentration of its aqueous solutions. Perhaps as a result of the loading of  $\text{H}_3\text{PO}_4$  on OS, the supernatant diluted and this facilitated the vaporization of water to dryness. For the dilute solutions, the solute–solvent interactions occurring in the bulk of the solution should be stronger than for the concentrated solution because of the smaller degree of  $\text{H}_3\text{PO}_4$  association, and this should have an unfavorable effect on the loading of  $\text{H}_3\text{PO}_4$  on OS.

Close inspection of the weight of carbon after washing compared after carbonization indicates that loaded phosphoric acid species were very sensitive to the subsequent washing. This was expected as the mass loss produced by washing of the OS-derived carbon with distilled water is attributable to lixiviation of phosphorus species, which are very polar ions/molecules and therefore highly soluble in water. Perhaps, the solution process was favored as a result of a decrease in the size of phosphorus species present in the OS carbon because of the carbonization process.

A slightly lower bulk density of activated carbon product was also observed at high phosphoric acid content due to the difference in the pore structure of the carbon product as discussed later on.

#### 3.2. Characterizing pore structure of the carbons

The shape of the adsorption isotherm can provide qualitative information on the adsorption process and the extent of the surface area available to the adsorbate. Fig. 1 shows the  $\text{N}_2$  adsorption–desorption isotherms at  $-196^\circ\text{C}$  of OS-based carbon prepared by phosphoric acid activation at different concentration. It is apparent that all isotherms of all carbon series belonging to type I according to the IUPAC classification (Sing et al., 1985), showing a significant increase in the adsorption at low  $P/P_0$  values ( $<0.1$ ), with barely defined knee and long plateau which extends to  $P/P_0 \approx 1.0$ , indicate that the ACFs are essentially microporous solids. An absence of hysteresis indicated the absence of mesoporosity, and suggested that the carbon products contained mostly micropores with only a small contribution of mesopore.

In the present investigation, although the adsorption isotherms for all samples are similar, the adsorption capacities are significantly different according to the  $\text{H}_3\text{PO}_4$  concentration. It was observed that increasing  $\text{H}_3\text{PO}_4$  concentration shifts the isotherm upward compared to that of other carbons.

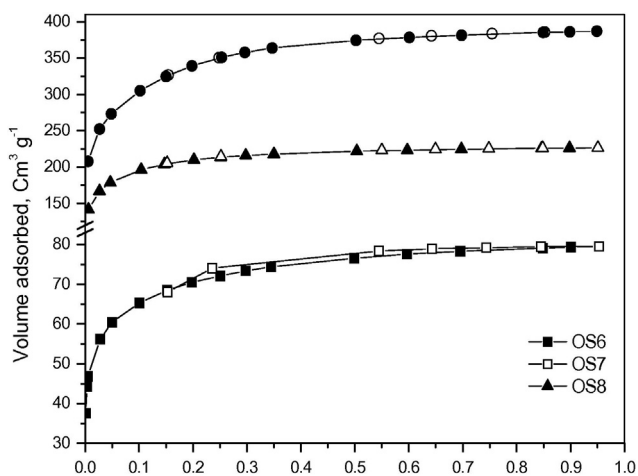
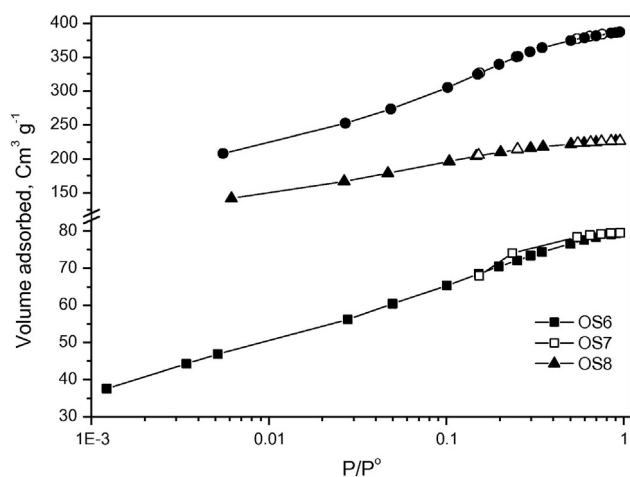
To take full advantages of the information provided by high-resolution nitrogen isotherm, these isotherms are represented on a semilogarithmic scale (Li et al., 1998). The adsorption isotherms expressed in a logarithmic pressure scale are often useful to investigate the differences in the structural properties especially at lower  $P/P_0$  region (Park and Jung, 2003). Adsorption processes can be divided into several distinct stages at relative pressures of  $10^{-6}$ – $10^{-4}$ ,  $10^{-4}$ – $10^{-2}$ ,  $10^{-2}$ – $10^{-1}$ ,  $0.1$ – $0.9$ , and  $0.9$ – $1.0$  which can be attributed to multiple stage pore filling processes (Ryu et al., 2000), such as: (i) filling of narrow micropores; (ii) monolayer formation on the surfaces of wider micropores such as supermicropores; (iii) filling of these wider micropores; (iv) monolayer formation and filling of mesopores by capillary condensation, and (v) filling of macropores by capillary condensation, which takes place at relative pressures close to unity.

Fig. 2 shows the adsorbed volume of  $\text{N}_2$  on the carbons vs. the logarithmic pressure. As seen from these semilogarithmic plots all samples show no uptake of nitrogen under a relative pressure of  $10^{-3}$ , indicating the presence of a few ultra micropores. There is significant uptake of nitrogen in the relative pressure range of  $10^{-3}$ – $10^{-1}$  indicating that all prepared samples have great part of its pores as super micropores and wider micropores.

The effect of acid concentration on the BET surface area, micropore, mesopore volume, and total pore volume are given in Table 2. The total pore volume,  $V_{\text{total}}$ , was calculated from nitrogen adsorption data as volume of liquid nitrogen at a relative pressure of 0.95. The micropore volume,  $V_{\text{micro}}$ , was determined by DR method, and the mesopore volume,  $V_{\text{meso}}$ , was obtained by the subtraction of micropore volume and total pore volume. As can be seen, the BET surface area and total pore volume increase with the increasing acid concentration. The increase in porosity with temperature can be attributed to the release of tars from cross-linked framework

**Table 1** Nomenclature, preparation conditions and yields of the activation procedure.

Carbon name	H <sub>3</sub> PO <sub>4</sub> (wt.%)	Carbonization temperature (°C)	Weight after impregnation (g)	Weight after carbonization (g)	Weight after washing/drying (g)	Bulk density (g/cm <sup>3</sup> )	Yield (%)
OS6	60	500	50.5	23.2	18.4	1.0	36.8
OS7	70	500	54	28.5	16.9	0.84	33.8
OS8	80	500	57	32.7	15.6	0.83	31

**Figure 1** Nitrogen adsorption isotherms for olive stone carbons.**Figure 2** Semi-logarithmic scale of nitrogen adsorption isotherms for olive stone carbons.

generated by the treatment of phosphoric acid (Hsu and Teng, 2000). The results are consistent with the findings of other workers (Molina-Sabio et al., 1995) who suggested that increasing the amount of phosphorus leads to an increase in the volumes of micro- and mesopores (table). The experimental data in Table 2 also show an increase in the average pore diameter with increasing concentration, showing that the development of porosity is also accompanied by a widening of the porosity as the amount of H<sub>3</sub>PO<sub>4</sub> is increased.

Similar effects of the amount of phosphoric acid on porosity development have been reported for other lignocellulosic precursors (Baquero et al., 2003; Molina-Sabio et al., 1995). It is generally accepted that the porosity is generated with phosphoric acid remaining intercalated in the internal structure of lignocellulosic materials. As the amount of H<sub>3</sub>PO<sub>4</sub> used increases, the volume filled by it and various polyphosphates will increase, resulting in larger pore volume and pore size.

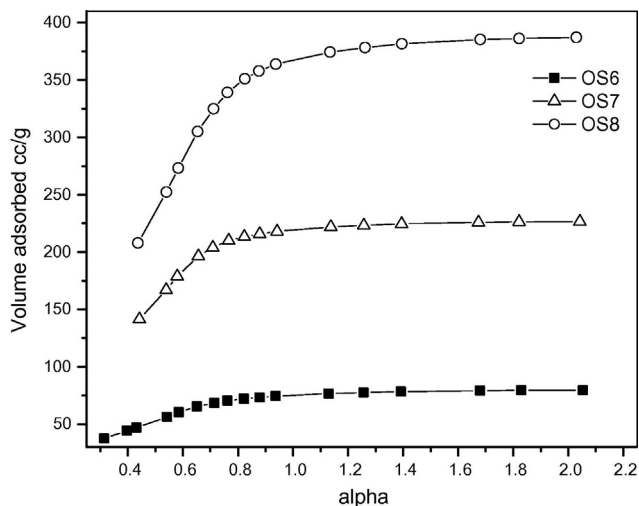
Fig. 3 shows  $\alpha_s$ -plots drawn from the isotherms in Fig. 1. It has been shown that the  $\alpha_s$ -plots of all activated carbons show two straight points (one for  $\alpha_s = 1.0$  and other for  $\alpha_s > 1.0$ ). The second linear section is almost parallel to the  $x$ -axis. This indicates the presence or absence of mesoporosity. The extension of the points at lower  $P/P_0$  values does not pass through the origin but cuts the  $y$ -axis for a positive value. This kind of deviation has been ascribed to the presence of narrow microporosity in these activated carbons (Seller-Perez and Martin-Martinez, 1991). Regarding the  $\alpha_s$ -plot analysis, Kaneko et al. (1992) found that the microporous carbon could show two upward swings from linearity below the downward bending due to saturated filling at higher  $\alpha_s$ , which they designated as filling swing FS and cooperative swings CS, corresponding to  $\alpha_s$  smaller and greater than 0.5, respectively. Both swings (FS and CS) come from enhanced adsorbent-adsorbate interaction as a function of the pore size and can be ascribed to different types of filling: FS results from primary micropore filling, which takes place in the ultramicropore (<0.8 nm) and CS results from cooperative adsorption in larger micropore (supermicropores of diameter > 1 nm). The  $\alpha_s$ -plot given in Fig. 3 shows that almost all samples show cooperative swings ( $0.5 < \alpha_s < 1$ ) with little evidence for filling swing ( $0 < \alpha_s < 0.5$ ) further confirming that wider micropores are the dominant pores in these samples.

Our results confirm the data obtained by (Terzyk et al. 2002) who studied the relation between DA-method parameters ( $E$  and  $n$ ) and concluded that carbon of the same  $n$  values show  $\alpha_s$ -plot with swings (FS or CS) depend on  $E$  values. In this concern, for high  $E$  values (> 30 kJ/mol) the obtained  $\alpha_s$ -plot belongs to the FS group. For  $E$  in the range 20–25 kJ/mol, the  $\alpha_s$ -plot belongs to the FS/CS-type. For the smallest energies, the  $\alpha_s$ -plot becomes the CS type. For our carbons  $n$  value of DA-method is 1.8 and the value of  $E$  is small (5.0–5.5 kJ/mol). Then the resultant  $\alpha_s$ -plot is CS type and nitrogen adsorption mechanism is related to the cooperative swing of secondary micropore filling (in supermicropores).

In our opinion, the picture of narrow microporosity from nitrogen adsorption is not obvious. There is lower cutoff of pore width less than two nitrogen molecule diameters (around 0.4 nm) is generally assumed for nitrogen adsorption at 77 K owing to restricted diffusion of nitrogen in narrow microporosity. Thus, it has been suggested that the adsorption of these

**Table 2** Pore structure parameters of olive stones carbons.

Carbon	$S_{\text{BET}}$ ( $\text{m}^2/\text{g}$ )	$r$ (nm)	$V_{\text{total}}$ (cc/g)	$V_{\text{micro}}$ (cc/g)	$V_{\text{meso}}$ (cc/g)
OS6	257	0.954	0.123	0.11	0.012
OS7	779	1.0	0.35	0.32	0.03
OS8	1218	1.1	0.6	0.5	0.1

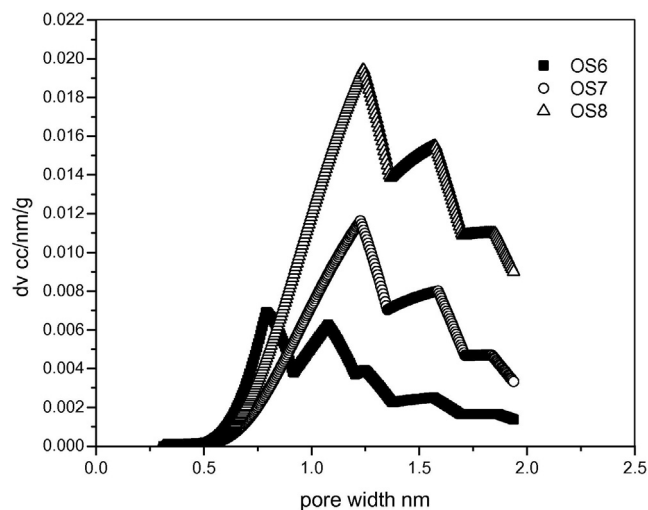
**Figure 3**  $\alpha$ -plot of various olive stones' carbon samples.

two molecules should be used in a complementary way in order to characterize microporosity more fully such as carbon dioxide adsorption. In this way, data obtained from nitrogen adsorption isotherms should only be taken as a qualitative estimation of the presence, to a lesser or larger extent, of narrow microporosity (Bello et al., 2002).

Bansal et al., (1988) have fit adsorption data for strongly activated and heterogeneous carbons with  $n$  values (of DA equation) between 1.5 and 2. For the activated carbons studied herein, it has been found that  $n$  is around 1.8. This indicates that carbons under study are strongly activated with great heterogeneous micropore structure.

The structural heterogeneity of porous material is generally characterized in terms of the pore size distribution. This pore size distribution represents a model of solid internal structure, which assumes that an equivalent set of non-interacting and regularly shaped model pores can represent the complex void spaces within the real solid (Ismadji and Bhatia, 2001). The pore size distribution is closely related to both kinetic and equilibrium properties of porous material and perhaps is the most important aspect for characterizing the structural heterogeneity of porous materials used in industrial application. The pore size distribution of the samples was evaluated by Horvath-Kawazoe (HK) method (Ustinov and Do, 2002). The HK pore size distribution of activated carbons studied is shown in Fig. 4.

The HK plots are in all cases bimodal, with two maxima centered around 0.8 and 1.0 nm for OS6 and shifted to new two peak maxima 1.2 and 1.6 for OS7 and OS8 with the increase of acid concentration. The predominant pore width indicates here that the presence of semicopore (diameter  $< 0.7$  nm) is not observed. OS8 exhibits larger values of

**Figure 4** H-K pore size distribution of olive stones activated carbon samples.

the micropore volumes, since the area under the HK curve is larger in this latter case. The fact that the pore size distribution plots show Downward end in the zone of the wider micropores close to the mesopores (i.e., around 2 nm) suggests no development of the mesoporosity in our samples.

### 3.3. External surfaces of resulting carbon using SEM

Scanning electron micrographs of the surface morphology of different samples of the activated carbons are given in Fig. 5. This figure shows the differences of the surface and porosity of the activated carbons prepared at 60wt.% and 70wt.%  $\text{H}_3\text{PO}_4$ . From these figures, it is obvious that the carbons produced at 60wt.% are non-porous carbons, while the activated carbons produced at 70wt.% have cavities and cracks on their external surfaces. It seems that the cavities on the surfaces of carbons resulted from the evaporation of the activating agent which in this case is phosphoric acid during carbonization, leaving the space previously occupied by the activating agent. The impregnation with  $\text{H}_3\text{PO}_4$  followed by a thermal treatment under inert atmosphere involves a remarkable degradation of the microstructure. Such degradation is coupled to relatively important mass losses. This mass effect becomes more and more noticeable as the acid increases, which results in a progressive decrease of the global yield of the process.

### 3.4. FTIR analysis

The carbon matrix does not consist of carbon atoms alone, but is also formed by other heteroatoms like hydrogen, oxygen,

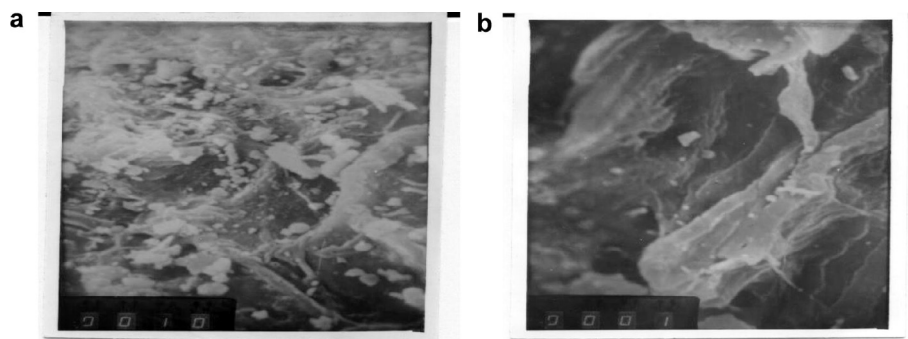


**Figure 5** Scanning electron microscope of OS6 (a) and OS7 (b).

nitrogen, halogen, sulfur, phosphorus, etc. These heteroatoms are bonded to the edges of the carbon layers, which govern the surface chemistry of the activated carbon.

Infrared spectroscopy provides information on the chemical structure of the carbon material. Fig. 6 shows FTIR spectra of the synthetic carbons obtained by phosphoric acid activation at different concentrations. All spectra show a wide transmittance band at  $3200\text{--}3600\text{ cm}^{-1}$  with a maximum at about  $3420\text{--}3440\text{ cm}^{-1}$ . This band can be assigned to the O–H stretching mode of hydroxyl groups and adsorbed water. The position and asymmetry of this band at lower wave numbers indicate the presence of strong hydrogen bonds (from carboxyls, phenols or alcohols) (Solum et al., 1995). A weak sharp transmittance band at  $3733\text{ cm}^{-1}$  present in spectra of all carbons and decreasing in carbons treated with high  $\text{H}_3\text{PO}_4$  concentration (OS7 and OS8). This peak may be ascribed to isolated O–H groups.

The FTIR spectrum of synthetic carbons OS6 and OS8 shows absorption bands due to aliphatic ( $2921$  and  $2855\text{ cm}^{-1}$ : C–H stretching in  $-\text{CH}_2-$ ;  $1450\text{ cm}^{-1}$ :  $-\text{CH}_2-$  deformation). In Fig. 6, the bands at  $885$ ,  $840$ , and  $775\text{ cm}^{-1}$  are due to out-of-plane deformation mode of C–H for different substituted benzene rings. The small band at about  $1700\text{ cm}^{-1}$  is usu-

ally assigned to C=O stretching vibrations of ketones, aldehydes, lactones or carboxyl groups.

The spectra of the prepared activated carbons also show a strong band at  $1600\text{--}1580\text{ cm}^{-1}$  due to C–C vibrations in aromatic rings. Broad band at  $1000\text{--}1300\text{ cm}^{-1}$  (maxima at  $1190\text{--}1200\text{ cm}^{-1}$ ) is usually found with oxidized carbons and has been assigned to C–O stretching in acids, alcohols, phenols, ethers and/or esters groups (Zawadzki, 1989). Nevertheless, it is also a characteristic of phosphorous and phosphor carbonaceous compounds present in the phosphoric acid activated carbons (Puziy et al., 2002). Assignment in this region is difficult because absorption bands are overlapped. The peak at  $1190\text{--}1200\text{ cm}^{-1}$  may be also assigned to the stretching mode of hydrogen-bonded P=O, to O–C stretching vibrations in P–O–C (aromatic) linkage and to P=OOH (Puziy et al., 2002). The shoulder at  $1100\text{ cm}^{-1}$  was ascribed to ionized linkage P–O– in acid phosphate esters, and to symmetrical vibration in a P–O–P chain (Bourbigot et al., 1995). To conclude on IR characterization, the most important changes introduced by the increase of the acid concentration are the development of C–H vibrations (possibly because of the loss of oxygen at the surface of the carbon material) as well as the increase of phosphorous group content ( $\sim 1100\text{ cm}^{-1}$ ).

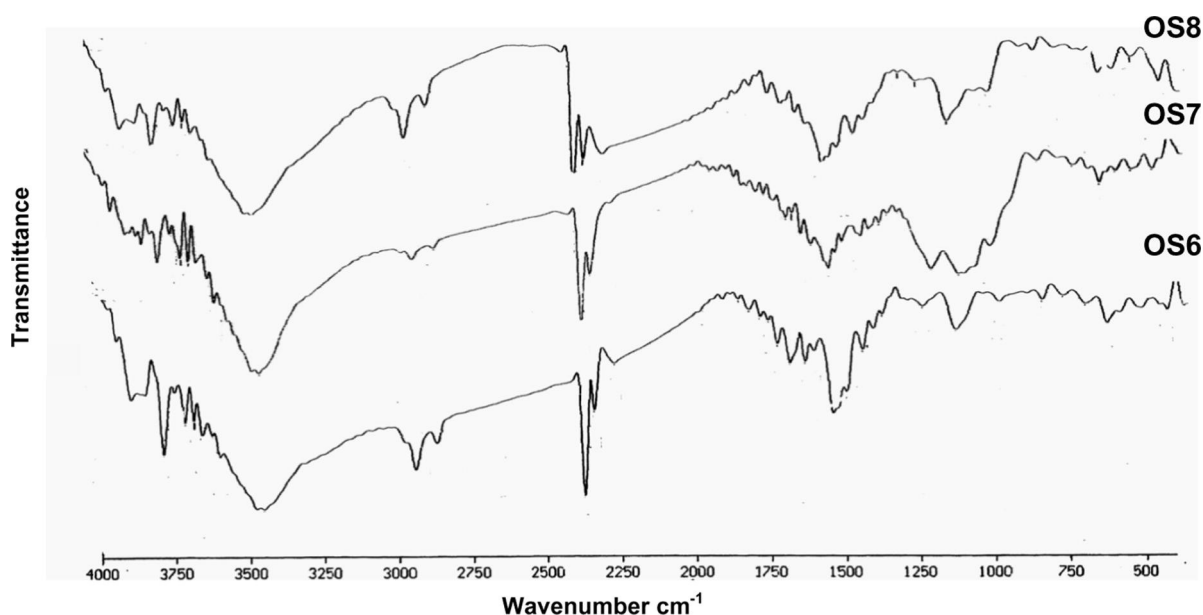


**Figure 6** FTIR spectra of activated olive stones at different  $\text{H}_3\text{PO}_4$  concentrations.

When concentrated  $\text{H}_3\text{PO}_4$  is mixed with date stones at high temperature, it appears to function both as an acid catalyst to promote bond cleavage reactions and formation of cross-links via processes such as cyclization and condensation and to combine with organic species to form phosphate and polyphosphate bridges that connect and crosslink biopolymer fragments (Jagtøyen and Derbyshire, 1998). Dastgheib and Rockstraw (2001) proposed that various surface acidic functional groups (oxygen- and/or phosphorus-containing groups) are developed through the surface oxidation as well as attachment of different oxygen/phosphorous groups to the surface, while developing required porosity. Benaddi et al. (1998) suggested that dehydration of cellulose by phosphoric acid is similar to dehydration of alcohols and at higher temperatures the phosphorous oxides act as Lewis acids and can form C–O–P bonds.

### 3.5. Fractal dimension of samples

Fractal analysis has become a new and powerful tool to describe the surface heterogeneity, geometric and structural properties of fractal surfaces and pore structures. The fractal dimension is the number used to quantify these properties: the larger the value of the surface fractal dimension, the more irregular and rougher the pore surface (Pyun and Rhee, 2004).

According to Frenkel, Halsey and Hill, a perfectly smooth surface has the fractal dimension of 2, whereas a very rough or irregular surface has the fractal dimension of 3. An activated carbon sample consists of very small crystallites such as graphite and disorganized carbon, because of the cross-linked structure between the crystallites. If activated carbon has a structure in which the crystallites are located parallel with respect to each other and has no cross-linked structure between the crystallites, then the fractal dimension is close to 2. On the contrary, if the crystallites are located in a disorderly manner and cross-linked structures develop, then the fractal dimension is close to 3. Thus, there is a close relationship between changes in the fractal dimension with that of the structure of activated carbon (Hayashi et al., 2002).

The  $D$  values obtained for all products prepared in this study are 2.95, 2.97 and 2.99 for OS6, OS7 and OS8, respectively. Increase in  $D$  values is observed as  $\text{H}_3\text{PO}_4$  concentration grows which is indicative of a development of the porous texture, with the increasing concentration of acid. Generally all samples have high values of fraction dimension near 3, which suggests that the surfaces are irregular and have strong micropore structures (Khalili et al., 2000).

## 4. Conclusions

Activated carbons with a well-developed pore structure are prepared from Olive stone by chemical activation with phosphoric acid. In general, as the phosphoric acid concentration increases the porous structure developed gives high surface and high total pore volume carbons.

## References

- Bansal, R.C., Donnet, J.B., Stoeckli, F., 1998. Active Carbon. Marcel Dekker, New York.
- Baquero, M.C., Giraldo, L., Moreno, J.C., Suárez-García, F., Martínez-Alonso, A., Tascón, J.M.D., 2003. Activated carbons by pyrolysis of coffee bean husks in presence of phosphoric acid. *J. Anal. Appl. Pyrolysis* 70, 779–784.
- Bello, G., Garcia, R., Arriagada, R., Sepulveda-Escribano, A., Rodriguez-Reinoso, F., 2002. Carbon molecular sieves from eucalyptus globulus charcoal. *Micropor. Mesopor. Mat.* 56, 139–145.
- Benaddi, H., Legras, D., Rouzaud, J.N., Beguin, F., 1998. Influence of the atmosphere in the chemical activation of wood by phosphoric acid. *Carbon* 36, 306–309.
- Bourbigot, S., Bras, M.L., Delobel, R., 1995. Carbonization mechanisms resulting from intumescence. II. Association with an ethylene terpolymer and the ammonium polyphosphate-pentaerythritol fire retardant system. *Carbon* 33 (3), 283–294.
- Dastgheib, S.A., Rockstraw, D.A., 2001. Pecan shell activated carbon: synthesis, characterization, and application for the removal of copper from aqueous solution. *Carbon* 39, 1849–1855.
- Diaz-Diez, M.A., Gomez-Serrano, V., Fernandez Gonzalez, C., Cuerda-Correa, E.M., Macias-Garcia, A., 2004. Porous texture of activated carbons prepared by phosphoric acid activation of woods. *Appl. Sur. Sci.* 238, 309–313.
- FAOSTAT, 2009. Website of Food and Agriculture organization of the United Nations. Available from: <<http://faostat.fao.org/>> .
- Halsey, G.D., 1948. *J. Chem. Phys.* 16, 93.
- Hayashi, J., Horikawa, T., Muroyama, K., Gomes, V.G., 2002. *Micropor. Mesopor. Mat.* 55, 63–68.
- Hsu, L.Y., Teng, H., 2000. Influence of different chemical reagents on the preparation of activated carbons from bituminous coal. *Fuel Process Technol.* 64, 155–166.
- Ismadji, S., Bhatia, S.K., 2001. Characterization of activated carbons using liquid phase adsorption. *Carbon* 39, 1237–1250.
- Jagtøyen, M., Derbyshire, F., 1998. Activated carbons from yellow poplar and white oak by  $\text{H}_3\text{PO}_4$  activation. *Carbon* 36, 1085–1097.
- Kaneko, K., Ishii, C., Ruike, M., Kuwabara, H., 1992. Origin of super high surface area and microcrystalline graphitic structures of activated carbons. *Carbon* 30, 1075.
- Khalili, N.R., Pan, M., Sandi, G., 2000. Determination of fractal dimensions of solid carbons from gas and liquid phase adsorption isothermes. *Carbon* 38, 573–588.
- Li, Z., Kruk, M., Jaroniec, M., Ryu, S.K., 1998. Characterization of structure and surface properties of activated carbon fiber. *J. Colloid. Interface Sci.* 204, 151–156.
- Matos, M., Barreiro, M.F., Gandini, A., 2010. Olive stone as a renewable source of biopolyols. *Ind. Crop. Prod.* 32, 7–12.
- Mehandjiev, D., Bekyarova, E., Nickolov, R., 1994. Micropore size distribution by a simplified equation. *Carbon* 32, 372–374.
- Molina-Sabio, M., Rodríguez-Reinoso, F., Caturia, F., Sellés, M.J., 1995. Porosity in granular carbons activated with phosphoric acid. *Carbon* 33, 1105.
- Niaounakis, M., Halvadakis, C.P., 2006. Olive Processing Waste Management: Literature Review and Patent Survey. Elsevier, Amsterdam.
- Nickolov, R., Mehandjiev, D., 2000. The simplified equation for micropore size distribution in adsorbents with different texture and chemical nature. In: *Proceeding of 9th International Symposium of Catalysis*, Varna, pp. 193–198.
- Nickolov, R.N., Mehandjiev, D.R., 1995. Application of the simplified equation for micropore size distribution to the study of water vapour adsorption on activated carbon. *Adsorpt. Sci. Technol.* 12, 203–209.
- Olivares-Marin, M., Fernandez-Gonzalez, C., Macias-Garcia, A., Gomez-Serrano, V., 2006. Preparation of activated carbon from cherry stones by chemical activation with  $\text{ZnCl}_2$ . *Sur. Sci.* 252, 5967–5971.
- Park, S.J., Jung, W.Y., 2003. KOH activation and characterization of glass fibers-supported phenolic resin. *J. Colloid. Interface Sci.* 265, 245–250.
- Prahas, D., Kartika, Y., Indraswati, N., Ismadji, S., 2008. Activated carbon from jackfruit peel waste by  $\text{H}_3\text{PO}_4$  chemical activation:

- Pore structure and surface chemistry characterization. *Chem. Eng. J.* 140, 32–42.
- Puziy, A.M., Poddubnaya, O.I., Martinez-Alonso, A., Suarez-Garcia, F., Tascon, J.M.D., 2002. Synthetic carbons activated with phosphoric acid I. Surface chemistry and ion binding properties. *Carbon* 40, 1493–1505.
- Pyun, S.-I., Rhee, C.-K., 2004. An investigation of fractal characteristics of mesoporous carbon electrodes with various pore structures. *Electrochim. Acta* 49, 4171–4180.
- Ryu, Z., Zheng, J., Whang, M., Zhang, B., 2000. Nitrogen adsorption studies of PAN-based activated carbon fibers prepared by different activation methods. *J. Colloid. Interface Sci.* 230 (2), 312–319.
- Seller-Perez, M.J., Martin-Martinez, J.M., 1991. *J. Chem. Soc. Faraday Trans.* 87, 1237–1243.
- Sing, K.S.W., Everett, D.H., Haul, R.A.W., Moscow, L., Pinerotti, R.A., Rouquerol, J., Siemieniowska, T., 1985. *Pure Appl. Chem.* 57, 603.
- Solum, M.S., Pugmire, R.J., Jagtoyen, M., Derbyshire, F., 1995. Evolution of carbon structure in chemically activated wood. *Carbon* 33, 1247–1254.
- Terzyk, A.P., Gauden, P.A., Kowalczyk, P., 2002. What kind of pore size distribution is assumed in the Dubinin–Astakhov adsorption isotherm equation? *Carbon* 40, 2879–2886.
- Timur, S., Kantarli, I.C., Ikizoglu, E., Yanik, J., 2006. Preparation of activated carbons from oreganum stalks by chemical activation. *Energ. Fuel* 20, 2636–2641.
- Ustinov, E.A., Do, D.D., 2002. Adsorption in slit-like pores of activated carbons: improvement of the Horvath and Kawazoe method. *Langmuir* 18, 4637–4647.
- Zawadzki, J., 1989. Infrared spectroscopy in surface chemistry of carbons. In: Throrer, P.A. (Ed.), . In: *Chemistry and Physics of Carbon*, vol. 21. Marcel Dekker, New York, pp. 147–386.